IIETA International Information and Engineering Technology Association
Advancing the World of Information and Engineering

Journal Européen des Systèmes Automatisés
Vol. 59, No. 10, October, 2026, pp. 2967-2977
Journal homepage: http://iieta.org/journals/jesa

A Novel DES-PRO Optimization Framework for Sub-THz STAR-RIS Networks Under Practical EM Coupling and Imperfect CSI

Rafal Azzam Abed

Department of Electrical Engineering, College of Engineering, University of Mosul, Mosul 41002, Iraq

Corresponding Author Email: rafal.azzam@uomosul.edu.iq

Copyright: ©2026 The author. This article is published by IIETA and is licensed under the CC BY 4.0 license (http://creativecommons.org/licenses/by/4.0/).

https://doi.org/10.18280/jesa.591017

Received: 21 August 2026
Revised: 13 October 2026
Accepted: 26 October 2026
Available online: 31 October 2026

Keywords:
6G wireless networks, sub-THz communications, simultaneously transmitting and reflecting reconfigurable intelligent surfaces channel state information, hardware impairments, Penalty-based Reformulation Optimization, Dynamic Energy Splitting

ABSTRACT

Sub-THz multi-user multiple-input multiple-output (MU-MIMO) networks in 6G offer high capacity with low latency. Yet, high frequencies suffer from severe signal propagation issues. To address this problem, simultaneous transmission and reflection reconfigurable intelligent surfaces (STAR-RIS) technology is applied to achieve full 360° coverage. Despite these advantages, practical deployment under the Energy Splitting (ES) protocol introduces complex non-convex optimization challenges, further exacerbated by non-linear amplitude-phase coupling, hardware impairments (HWIs), phase noise, and imperfect channel state information (CSI error ratio $\epsilon = 0.20$). To address these physical-layer bottlenecks, this paper proposes a robust, low-complexity optimization framework integrating Penalty-based Reformulation Optimization (PRO) with Block Coordinate Descent (BCD). By reformulating intricate amplitude-coupling constraints into objective penalty terms, the proposed scheme decomposes the joint active beamforming and passive response problem into efficient, iteratively updated computational blocks. The proposed framework achieves a peak sum rate of 72 bits/s/Hz with $N = 128$ under balanced user distributions at 35 dBm. Under a severe 30% link blockage, the Dynamic Energy Splitting-Penalty-based Reformulation Optimization (DES-PRO) algorithm maintains 53 bits/s/Hz, outperforming benchmark schemes by up to 32.5%. Furthermore, under imperfect CSI ($\epsilon = 0.15$), the system maintains a resilient throughput of 39.6 bits/s/Hz, proving its robustness against channel estimation errors.

1. INTRODUCTION

The rapid advances in today's wireless communication technologies are essential to meet the fast-growing number of users, which demands fast data rates and low latency. Fifth-generation (5G) networks represent a major shift in used frequencies, moving beyond microwave frequencies to operate within the high-frequency millimeter-wave (mmWave) band. The millimeter-wave band spans (30-300) GHz. The high frequency of these waves enables communication networks to achieve high transmission capacity gain and high-speed data throughput [1, 2].

Millimeter-wave communication systems face technical challenges and constraints related to radio signal propagation properties. Radio signal transmission in mmWave bands suffers heavily from free-space path loss, atmospheric absorption, and severe attenuation caused by rain and physical obstacles [3]. To mitigate these propagation issues and severe signal attenuation, beamforming techniques and massive multiple-input multiple-output (mMIMO) antenna architectures are employed. These technologies focus electromagnetic (EM) energy into narrow beams directed toward user devices rather than omnidirectional radiation [4]. These narrow beams increase the signal-to-noise ratio (SNR) and improve overall system efficiency [5].

Sixth-generation (6G) networks aim to provide ultra-fast data transfer rates along with full coverage of the propagation environment. However, the use of high frequencies makes signals prone to severe degradation in line-of-sight (LoS) paths when encountering obstacles. To overcome this problem, reconfigurable intelligent surface (RIS) technology has emerged to redirect wave propagation paths. This surface technology helps reduce interference and improve spectral efficiency compared to earlier wireless systems [6, 7].

Reconfigurable intelligent surfaces (RIS) represents an excellent solution to overcome signal loss problems in the propagation environment and achieve high energy efficiency (EE) in MIMO systems. The additional pilot signal overhead has been addressed using compressive sensing techniques, such as the SOMP algorithm for channel estimation [8]. Ensuring physical layer security plays a key role in countering signal jamming and data poisoning [9]. Moreover, deep learning models such as the IRS-DRCEN and IRS-CorNet architectures have been proposed for channel state information (CSI) estimation in IRS-aided massive MIMO systems [10]. Furthermore, merging RIS beamforming with deep neural networks (DNNs) boosted the Signal-to-Interference-plus-Noise Ratio (SINR) by up to 27.5% [9].

Recent research on 5G and 6G networks operating in mmWave and sub-THz bands addresses the blockages caused by physical obstacles, such as solid walls [11]. To overcome this limitation, simultaneously transmitting and reflecting

reconfigurable intelligent surfaces (STAR-RIS) have been introduced [11, 12]. STAR-RIS technology outperforms conventional reflecting-only RIS, which offers a coverage span limited to 180° [12]. STAR-RIS achieves complete 360° coverage by allowing every surface element to reflect and transmit incident signals at the same time [12, 13]. This capability gives the surface added degrees of freedom (DOF) to adjust both phase and amplitude responses [13]. As a result, reliable links are established for users located both in front of and behind the surface, all while using minimal power [12, 13]. eploying STAR-RIS faces physical layer challenges caused by hardware impairments (HWIs), phase errors, and pilot contamination under non-ideal channel conditions [14]. Using the energy splitting (ES) protocol (where each element splits power between transmission and reflection) makes signal optimization highly complex [15, 16]. To address these obstacles, this study provides solutions to reduce non-linear signal distortion by presenting an optimization framework that integrates two algorithms: Penalty-based Reformulation Optimization (PRO) and Dynamic Energy Splitting (DES). This research proposes a novel algorithm to solve the coupled phase and amplitude physical constraints, optimizing the STAR-RIS system under the ES protocol [17]. The reformulation enables the application of the Block Coordinate Descent (BCD) algorithm to decompose the optimization problem into independent computational blocks, sequentially updating the active beamforming vector at the Base Station (BS) and the passive phase-amplitude response at the intelligent surface in a direct, iterative manner, thereby eliminating the excessive computational complexity associated with conventional Alternating Optimization (AO) methods [18]. The proposed Dynamic Energy Splitting-Penalty-based Reformulation Optimization (DES-PRO) framework is engineered to tackle potential impairments in sub-THz channels by operating as a dynamic optimization mechanism for wireless networks, moving beyond static network evaluation. Utilizing the available Channel State Information (CSI), the framework iteratively updates the system control variables through joint active beamforming at the BS and passive amplitude-phase control across the STAR-RIS. This strategy achieves intelligent system resource management while respecting practical EM constraints, thereby establishing a direct bridge between wireless physical-layer metrics and dynamic automated system control.

The primary scientific contributions of this paper are fourfold:

1. Proposing a practical system model that integrates non-linear EM amplitude-phase coupling in STAR-RIS elements, taking into account 300 GHz molecular absorption and channel estimation errors (imperfect CSI).

2. Developing and using the DES-PRO algorithm within an optimization framework that decouples joint active and passive beamforming and converts non-convex constraints into penalty functions.

3. Devising a dynamic full-power mode-switching strategy to reliably restore connectivity under severe link blockages.

4. Validating network stability under CSI estimation errors up to 25%, while demonstrating sum-rate improvements of up to 32% compared to benchmark methods.

2. LITERATURE REVIEW

Because RIS can adjust the reflection and refraction of incoming signals, prior research highlighted them as a critical technology for EM propagation. Nevertheless, their structural architecture limits their operational coverage to a 180° area. To achieve broader coverage STAR-RIS technology was employed in the study [19] showed that using the energy-splitting (ES) protocol provides high DOF and operational flexibility. However, that study assumed ideal user hardware alongside non-ideal channel models. It overlooked the degradation caused by HWIs and phase noise at high frequencies. Furthermore, this study [20] introduces a STAR-RIS model for various hardware parameters, mitigating pilot contamination (reusing the same pilot sequence among multiple users) and phase errors in MIMO and Massive MIMO networks. A mathematical model was developed operating under a time-division duplexing (TDD) system and the ES protocol, considering users distributed across both the transmission and reflection regions of the surface. The authors derived the linear minimum mean-square error (LMMSE) channel estimate and evaluated the spectral efficiency for two cell-free massive MIMO (CF-mMIMO) systems: one using a conventional surface and the other assisted by STAR-RIS. Numerical results across different hardware parameters demonstrated that the STAR-RIS-assisted system achieves a 95%-likely spectral efficiency that is 14.7 times higher than that of conventional systems.

To evaluate HWIs and signal blockage, the study [21] utilizes RIS technology to mitigate link obstructions through a swarm intelligence-based optimization algorithm. By employing a 304.2 GHz carrier frequency for THz signals to evaluate the outage probability, the results demonstrated that expanding the number of surface elements from 40 to 80 reduces the outage probability by 97% while increasing ergodic capacity by 25%.

In light of using conventional RIS (180°) and for the purpose of studying the coupling between phase shift and amplitude, the researchers [22] presented a study in this field by breaking the ideal concept. The researchers worked on optimizing the beamforming matrix by employing Active Beamforming to achieve a high SINR. Two scenarios were utilized with two algorithms for each scenario; the first: the AO algorithm and the Penalty-Based algorithm in the single-user case, and the second: the Extended Penalty-Based algorithm and the Two-Stage algorithm for multiple users. Through the implementation of these algorithms, the results proved that the maximum amplitude is achieved at distant angles ($-\pi, \pi$) and the minimum at a zero angle as it absorbs energy. Although the study considered the phase-dependent amplitude response, it did not investigate CSI estimation errors in the sub-THz frequency range.

The authors provided in the study [23] a realistic wireless link evaluation for RIS models in the 140 GHz band. Hardware imperfection models were incorporated, including angular coverage where a 60° angle induces a 3 dB loss phase resolution, proving that 2 bits is optimal, as well as aperture efficiency and beam squinting, where a 3 dB frequency drop occurs with shifts in beam direction. The link budget for received power was calculated at 20 meters for the indoor scenario and 100 meters for the outdoor scenario. The study demonstrated that accounting for hardware imperfections and beam squinting is imperative when investigating sub-THz frequencies. In response to the severe computational complexity inherent in non-convex optimization for intelligent surface-assisted networks, recent literature has focused on developing robust iterative algorithms. In this study [24], the

authors investigated hardware imperfections alongside statistical Channel State Information (S-CSI) to reduce computational complexity. The study addressed users located in both the front and back spaces of the STAR-RIS. To optimize the ES protocol and the Mode Switching (MS) protocol, the Projected Gradient Ascent Method (PGAM) was employed for joint amplitude and phase optimization. The results demonstrated that increasing the number of surface elements mitigates the impact of hardware imperfections. The study did not investigate HWIs under CSI in the sub-THz frequency range, nor did it incorporate a nonlinear EM amplitude–phase coupling model.

In this study [25], the authors discussed a NOMA-based multiple access scheme operating at conventional frequencies with a STAR-RIS providing full-space coverage for users. Three surface operating protocols were considered: ES, MS, and Time Switching (TS). To achieve structural system optimization, the BCD algorithm and the AO framework were employed. The study assumed decoupled, non-ideal phase and amplitude, along with HWIs. To evaluate the EE for users located on both sides of STAR-RIS, the authors [26] employed an AO framework. By leveraging the general inertial projected gradient (GIPG) algorithm in conjunction with fractional programming (FP), the complex optimization problem was effectively resolved under the assumption of perfect CSI. Nevertheless, the study omitted the non-linear phase-dependent amplitude coupling model. The study did not investigate channel estimation errors or the EM coupling between amplitude and phase.

Researchers [27] addressed the issue of reduced transmit power reaching users when using STAR-RIS surfaces. By applying the ES protocol, they optimized both amplitude and phase. The proposed algorithm with independent amplitude achieved a transmit power of 27.1 dBm within 7 to 8 iterations, while the equal-amplitude setup required 4 iterations at 26.4 dBm. The fixed-phase configuration stabilized at 29.2 dBm after approximately 8 iterations, whereas the conventional surface required 5 iterations to stabilize at 31.5 dBm. In analyzing transmit power against the threshold, the algorithm attained 21.2 dBm at 15 dB and 30.5 dBm at 25 dB. Regarding the impact of increasing the number of surface elements, the transmit power decreased by 9.7 dBm. However, the study relied on conventional channel models rather than sub-THz frequencies. Furthermore, it assumed perfect channel conditions and analyzed amplitude and phase independently without coupling them.

3. SYSTEM MODEL

To explicitly bridge the physical layer communication with automated system optimization, the proposed DES-PRO algorithm dynamically regulates system parameters through a closed-loop framework across three distinct stages: System State Update: It continuously adapts to time-varying channel dynamics while explicitly accounting for non-ideal channel estimation errors ($\epsilon = 0.2$) to maintain robust communication quality, Iterative Control Calibration: It adjusts the system control variables at each iteration to ensure seamless tracking of system states and Dynamic Resource Allocation: It dynamically optimizes power splitting between transmission and reflection via the DES protocol, thereby maximizing the total sum-rate while satisfying realistic coupled EM constraints. The interaction between DES and PRO is orchestrated through a BCD framework. Specifically, the DES module determines the global energy allocation between users located in the transmission and reflection zones, whereas the PRO module manages the practical phase-amplitude coupling constraints. Within this framework, the BCD procedure sequentially updates the system variables at the BS, ensuring seamless joint optimization through this alternating iterative process. Simultaneously, Transmitting and Reflecting Intelligent Surfaces (STAR-RIS) represent a paradigm shift in intelligent surface design due to their capability to overcome the half-space coverage limitations of conventional intelligent surfaces and provide full-space 360° coverage [12]. The mathematical core of research in this technology centers on handling the coupled physical phase-shift constraints between transmission and reflection modes [18], alongside the development of joint beamforming algorithms operating under interference-limited multi-user environments [27-29]. These coupled physical-layer characteristics lead to challenging non-convex optimization problems that require efficient iterative optimization techniques [28, 29]. The following section provides a detailed mathematical formulation of the system models and optimization algorithms developed to address these coupled physical-layer challenges.

$$\begin{aligned}\theta_t(t) &= diag\big(\beta_{t,1}(t)e^{j\emptyset_{t,1}(t)}, \beta_{t,2}(t)e^{j\emptyset_{t,2}(t)}, \\ &\quad \dots, \beta_{t,N}(t)e^{j\emptyset_{t,N}(t)}\big) \in C^{NxN} \\ \theta_r(t) &= diag\big(\beta_{r,1}(t)e^{j\emptyset_{r,1}(t)}, \beta_{r,2}(t)e^{j\emptyset_{r,2}(t)}, \\ &\quad \dots, \beta_{r,N}(t)e^{j\emptyset_{r,N}(t)}\big) \in C^{NxN}\end{aligned} \quad (1)$$

where, $\theta_t(t), \theta_r(t)$ represent the transmission and reflection response matrices of the STAR-RIS at time index t, respectively. The scalar N denotes the total number of STAR-RIS elements, while diag(.) transforms a vector into its corresponding diagonal matrix. Furthermore, the parameters $\beta_{t,n}(t)$, $\beta_{r,n}(t) \in [0, 1]$ represent the amplitude adjustment coefficients for the transmitted and reflected signals via the nth element at time index t, respectively. Similarly, $\emptyset_{r,N}(t)$, $\emptyset_{t,N}(t) \in [0, 2\pi)$ denote the phase shifts applied to the transmitted and reflected signals by the nth element at time index t, where, j = $\sqrt{-1}$ is the imaginary unit [30].

To ensure strict compliance with physical energy conservation laws and EM coupling constraints [30]:

$$\beta_{t,n}^2(t) + \beta_{r,n}^2(t) \leq 1, n \in \{1, \dots, N\} \quad (2)$$

The passive EM and circuit dynamics of the intelligent surface elements enforce a tight coupling between the transmission and reflection phase shifts at the nth element. Because the transmitted and reflected signals share common internal hardware components within each element, their phase responses cannot be dynamically configured independently. To capture this physical coupling regime where the reflection phase shift is deterministically governed by the selected transmission phase shift, this constraint is formulated using the cosine-orthogonality condition, enforcing a fixed relative phase difference of either $\pi/2$ or $3\pi/2$ (90° or 270°) according to the following equation [30]:

$$\cos\left(\emptyset_{t,n}(t) - \emptyset_{r,n}(t)\right) = 0 \; \forall n \epsilon \{1,2, \dots N\} \quad (3)$$

where, $\emptyset_{t,n}(t) \in [0,2\pi)$, $\emptyset_{r,n}(t) \in [0,2\pi)$ denote the transmission and reflection phase shifts of the n-th STAR-RIS

element at time slot t, respectively, and N is the total number of surface elements. This condition implies that $|\phi_{t,n}(t) - \phi_{r,n}(t)| \in \left\{\frac{\pi}{2}, \frac{3\pi}{2}\right\}$.

To evaluate the communication performance and assess the received signal quality for each user within the network, the instantaneous SINR is formulated. This expression quantifies the desired signal power delivered to the kth user via the combined direct link and the cascaded STAR-RIS link, scaled against the aggregate interference power originating from signals destined for other co-channel users alongside the thermal noise power at the receiver. The SINR is formulated based on the channel model adopted from [30, 31]. The instantaneous SINR is mathematically defined as follows.

$$SINR_k(t) = \frac{\left|\left(h_{r,k}^H \theta_v(t) G + h_{d,k}^H\right) W_k(t)\right|^2}{\sum_{m \neq k}\left|\left(h_{r,k}^H \theta_v(t) G + h_{d,k}^H\right) W_m(t)\right|^2 + \delta_k^2} = v \in \{t, r\} \quad (4)$$

where, the instantaneous SINR for user k is represented by $SINR_k(t)$. The symbol $h_{r,k}^H$ denotes the complex wireless channel vector between the STAR-RIS surface and user k, while $h_{d,k}^H$ represents the direct channel vector between the BS and user k. The notation $\theta_v(t)$ refers to the dynamic surface response matrix of the intelligent surface at time slot t for operational mode v, where, $v = t$ denotes signal transmission (refraction) and $v = r$ denotes reflection. Furthermore, G represents the aggregate wireless channel matrix between the BS and the STAR-RIS. The symbol $W_k(t)$ designates the digital beamforming vector synthesized by the BS for user k at time slot t, where, $W_m(t)$ represents the beamforming vector allocated to interfering users ($m = k$), which induces co-channel interference on user k. The parameter δ_k^2 models the Additive White Gaussian Noise (AWGN) power at the receiver of user k. The term $\sum_{m=k}|.|$ accounts for the aggregate interference power resulting from all other interfering users. Finally, $v \in \{t, r\}$ indicates the element operational mode assigned to the user (t for transmission and r for reflection). Consequently, the achievable data rate is calculated via the following equation [32]:

$$R_{sum}(t) = \sum_{k=1}^{K} B \log_2(1 + SINR_k(t)) \quad (5)$$

To bridge the gap between theoretical models and practical applications of intelligent surfaces, the practical phase-shift model is adopted. This model overcomes the simplified assumption that phase shift and amplitude can be controlled independently. In practical passive intelligent surfaces, changing the phase shift is inherently associated with a nonlinear variation in the reflection amplitude due to the characteristics of the electronic circuits used in practical implementation. To represent the effectiveness of the nonlinearity between amplitude and phase using the DES-PRO algorithm through the following mathematical relationship [22, 33]:

$$\beta_n^v(\phi_n^v) = (1 - \beta_{min})\left(\frac{sin(\phi_n^v - \phi_0) + 1}{2}\right)^{\gamma} + \beta_{min} v \in \{t, r\} \quad (6)$$

The mathematical symbols used in the equation indicate the following:

$\beta_n^v(\phi_n^v)$: the effective amplitude adjustment which dependent on phase shift ϕ_n^v.

t, r: symbols indicating discrete time slot and transmission respectively and $v \in \{t, r\}$: operation mode.

ϕ_0: the Circuit reference phase shift.

γ: the intensity of the EM response (it measures changes in amplitude relative to changes in phase).

β_{min}: represents the minimum amplitude attenuation coefficient ($\beta_{min:} \in [0,1]$).

To study the effect of disconnection between the proposed STAR-RIS surface and the users using $\beta_n^v(\phi_n^v) \in [\beta_{min}, 1]$.

To study the practical case of channel estimation in communication systems by considering channel estimation imperfections, according to the following equation [34, 35]:

$$G = \hat{\mathrm{G}} + \Delta G, \qquad .s.t \|\Delta G\|_F \leq \epsilon \left\|\hat{\mathrm{G}}\right\|_F \quad (7)$$

where, G represents the actual complex wireless channel matrix between the BS and the STAR-RIS, where, $\hat{\mathrm{G}}$ denotes the estimated channel matrix acquired at the BS. The matrix ΔG models the practical channel estimation error modeled as $\Delta G = \epsilon \frac{\|\hat{\mathrm{G}}\|_F}{\|Z\|_F} Z$, where, Z is zero mean a Gaussian random matrix. The notation $\|.\|_F$ designates the Frobenius norm, used to measure the aggregate magnitude of the channel estimation error, while ϵ denotes the upper bound on the allowable channel error ratio, set to $\epsilon = 0.20$ to represent a 20% estimation error level.

The DES algorithm addresses the optimization problem of continuously updating the amplitude and phase values across the dynamic STAR-RIS surface. The algorithm operates by generating and updating the continuous phase vector $\phi_t = [\phi_1, \ldots, \phi_N]^T$, while strictly satisfying the power conservation constraints via adaptive gradient scaling [36, 37].

$$\phi^{(k+1)}(t) = P_{\phi}\left(\phi^{(k)}(t) + \alpha_k \nabla_{\phi} R_{sum}\left(\phi^{(k)}(t), w^{(k)}(t)\right)\right) \quad (8)$$

The phase shift vector for all intelligent surface elements at iteration index k during time slot t is denoted by $\phi^{(k)}(t)$. The scalar α_k represents the adaptive step-size parameter at iteration step k. Furthermore, $\nabla_{\phi} R_{sum}(.)$ designates the gradient of the sum-rate objective function evaluated with respect to the phase shift vector. To guarantee that the phase angles are constrained within the feasible region [0, 2π), the projection operator is denoted by $P_{\phi}(.)$, which explicitly enforces the mandatory cosine-orthogonality condition satisfying $\left|\phi_{t,n} - \phi_{r,n}\right| \in \left\{\frac{\pi}{2}, \frac{3\pi}{2}\right\}$.

Meanwhile, the PRO algorithm addresses the complex non-linear coupling problem and mode-switching mechanism by leveraging Quadratic Fractional Programming (QFP) decomposition and block-coordinate optimization [18, 22, 38]. To calculate the optimal amplitude distribution vector during the (k+1) by the following subproblem:

$$\beta^{(k+1)}(t) = \arg min_{\beta(t) \in B} \left\|W^{(k)}(t) - F_{PRO}(\beta_{(t)}, \phi^{(k)}(t)\right\|_F^2 + \lambda D_{EM}(\beta_{(t)}, \phi^{(k)}(t)) \quad (9)$$

where, $\beta_{(t)}$ represents the aggregate transmission and reflection amplitude vector at time slot t, which is expressed

as follows:

$$\beta_{(t)} = (\beta_{t,1}, \dots., \beta_{t,N}(t)), (\beta_{r,1}, \dots., \beta_{r,N}(t))$$

where, β denotes the feasible constraint set spanning all available transmission and reflection amplitudes within the vector $\beta_{(t)}$, whether defined via continuous bounds $\beta_n^v(t) \in [0,1]$ or binary discrete modes $\beta_n^v(t) \in [\beta_{min}, 1]$ under full blockage recovery scenarios, $n \in \{1,2,\dots,N\}$ and $v \in \{t,r\}$. $W^{(k)}(t)$ is the digital beamforming weight matrix at iteration k. The operator $F_{PRO}(.)$ represents the transformation mapping function that couples the amplitude matrix with the digital beamforming weights w. Furthermore, the scalar λ designates the penalty parameter, where, $D_{EM}(.)$ defines the metric function measuring deviation from the practical physical EM coupling curve of the surface elements $\beta_n^v(\phi_n^v)$.

To contextualize the scientific contribution of this study, the overall optimization problem is formulated by incorporating all physical and realistic operational constraints. This is sequentially addressed by the iterative operator of the proposed DES-PRO algorithm, as detailed in the following joint equation:

$$\max_{W(t),\phi(t),\beta(t)} R_{sum}\big(W(t), \phi(t), \beta(t)\big) s.t. \mathcal{C}_1, \mathcal{C}_2, \mathcal{C}_3, \mathcal{C}_4 \quad (10)$$

where, the iterative optimization problem is solved via the following coupled subproblems:

$$W^{(K+1)}(t), \phi^{(K+1)}(t),\ \beta^{(K+1)}(t)) = \mathcal{T}_{DES-PRO}\big((W^{(K)}(t), \phi^{(K)}(t),\ \beta^{(K)}(t) \big| \hat{\mathrm{G}}, \epsilon)\big)$$

where, constraints $\mathcal{C}_1$ through $\mathcal{C}_4$ are defined as follows:

1. $\mathcal{C}_1$ is the total transmit power budget at the BS, requiring the aggregate power of the digital beamforming vectors not to exceed the maximum allowable power threshold as formulated by [39]:

$$\sum_{k=1}^{K} \|w_k(t)\|^2 \le P_{max}$$

2. $\mathcal{C}_2$ is dynamic power conservation across each element of the surface, requiring the sum of the transmission and reflection power response squares not to exceed unity, as expressed by [30]:

$$\beta_{t,n}^2(t) + \beta_{r,n}^2(t) \le 1$$

3. $\mathcal{C}_3$ is dictates the physical phase coupling condition, expressed as follows [30]:

$$\left|\phi_{t,n}(t) - \phi_{r,n}(t)\right| \in \{\frac{\pi}{2}, \frac{3\pi}{2}\}$$

4. $\mathcal{C}_4$ represents the imperfect channel estimation error bound, given by equation $\|\Delta G\|_{\mathrm{F}} \le \epsilon \|G\|_{\mathrm{F}}$ in which the error parameter value is set to $\epsilon = 0.2$ [35].

The notation $\mathcal{T}_{DES-PRO}$ denotes the joint iterative operator of the proposed DES-PRO algorithm, which updates the system state from iteration k to state $k+1$. Furthermore, P_{max} represents the maximum allowable transmit power budget at the BS, $\hat{\mathrm{G}}, \epsilon$ denotes the estimated channel matrix.

To trace the iterative optimization steps of the proposed algorithm through Algorithm 1.

Algorithm 1: Proposed DES-PRO Iterative Optimization Framework

Input: Estimated channel matrix $\hat{\mathrm{G}}$, channel error bound ϵ, maximum transmit power $P_{\max}$, number of STAR-RIS elements N, maximum iterations $K_{\max}$, and convergence tolerance ε_{th} .Initialization: Set iteration counter $k = 0$; initialize active beamforming matrix $\mathrm{W}^{(0)}$, STAR-RIS phase shifts $\phi^{(0)}$, amplitude vector $\beta^{(0)}$, and penalty parameter $\lambda^{(0)}$.

1: Repeat

2: Step 1 (Digital Active Beamforming Optimization): Update $\mathrm{W}^{(k+1)}$ by maximizing the achievable sum-rate objective R_{sum} subject to power constraint (C1), while keeping $\phi^{(k)}$ and $\beta^{(k)}$ fixed.

3: Step 2 (DES Phase Shift Updating via Gradient Projection): Compute the updated phase shift vector using Eq. (8):

$$\phi^{(k+1)} = P_{\phi}\left(\phi^{(k)} + \alpha_k \nabla_{\phi} R_{\text{sum}}\left(\phi^{(k)}, \mathrm{W}^{(k)}\right)\right)$$

subject to the coupled phase constraint $|\phi_{t,n} - \phi_{r,n}| \in \left\{\frac{\pi}{2}, \frac{3\pi}{2}\right\}$ for all $n = 1, \dots, N$.

4: Step 3 (PRO Amplitude Vector Reformulation Optimization): Compute the updated amplitude vector using Eq. (9):

$$\beta^{(k+1)} = \arg\min_{\beta \in \mathcal{B}} \left\|\mathrm{W}^{(k)} - F_{\text{PRO}}\left(\beta, \phi^{(k)}\right)\right\|_F^2 + \lambda^{(k)} D_{\text{EM}}\left(\beta, \phi^{(k)}\right)$$

5: Step 4 (Penalty Scaling and Iteration Increment): Update the penalty multiplier $\lambda^{(k+1)}$, evaluate the updated objective function value, and set $k \leftarrow k + 1$.

6: Until the convergence criterion is satisfied or $k = K_{\max}$.

Output: Optimal active beamforming matrix W^*, optimal phase shift vector ϕ^*, and optimal amplitude vector β^*.

4. SIMULATIONS AND RESULTS

4.1 Simulation parameters

The performance evaluations of the proposed DES-PRO framework for a multi-user multiple-input multiple-output (MU-MIMO) system operating in the sub-THz spectrum are conducted via MATLAB-based numerical simulations. The underlying network architecture comprises a BS deployed with a uniform linear array (ULA) to serve multiple single-antenna users through a wideband multi-carrier scheme, assisted by a STAR-RIS platform [38, 39]. To guarantee physical accuracy, the non-linear EM amplitude-phase coupling constraints at the STAR-RIS interface are strictly incorporated into the model [22, 33]. Furthermore, imperfect CSI is modeled over Rician fading channel conditions to faithfully emulate real-world propagation environments [38]. The primary simulation parameters and system configurations are summarized in Table 1 [38, 39].

Table 1. The simulation parameters used

Parameters	Value
Carrier Frequency	300 GHz
BS Transmit Antennas	8
STAR-RIS Elements	32, 64, 128
Number of Users	2-16
Number of Subcarriers	16
BS Transmit Power	35 (sweep: 20-35 dBm)
Noise Power Spectral Density	-90 dBm
CSI Error Bound Ratio	0.2 (sweep: 0-0.25)

Note: Base Station (BS); reconfigurable intelligent surface (RIS); channel state information (CSI).

4.2 Electromagnetic coupling and THz channel characteristics

To capture realistic physical deployment scenarios, Figure 1 illustrates the hardware constraints and signal propagation characteristics incorporated into the sub-THz wideband STAR-RIS simulation environment.

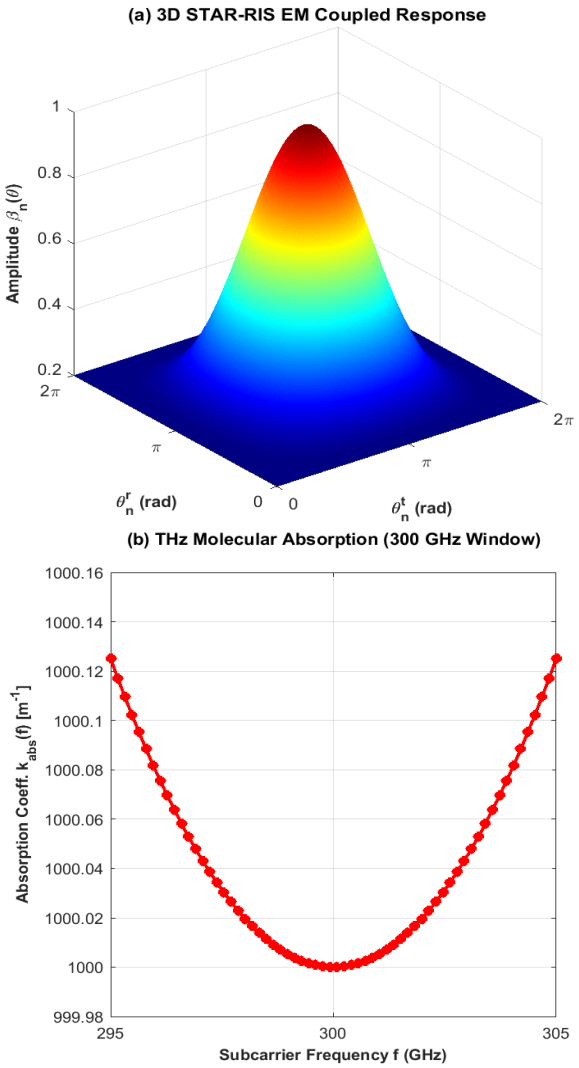


Figure 1. Characterization of system physical dynamics: (a) 3D electromagnetic (EM) coupled amplitude-phase response of simultaneously transmitting and reflecting reconfigurable intelligent surfaces (STAR-RIS), (b) Terahertz molecular absorption coefficient around 300 GHz

Figure 1(a) illustrates the non-ideal 3D electromagnetic response between amplitude and phase $\beta_n(\theta)$, for the nth element of the STAR-RIS surface as a function of the transmission and reflection phase shift angles ($\theta_n^r, \theta_n^r \in [0, 2\pi)$. Conventional algorithms for RIS in literature are typically designed under ideal hardware assumptions that presuppose a constant full amplitude ($\beta_n = 1$), regardless of the phase shift value. The surface plot above demonstrates the presence of strong non-linear electromagnetic coupling, wherein the achieved amplitude reaches its maximum value of $\beta_n = 1$ only within a narrow phase region, while severely degrading down to $\beta_n = 0.2$ in other regions. This emphasizes the direct necessity of the proposed DES mechanism, which inherently accounts for this non-ideal coupling from the outset to jointly optimize the transmission and reflection phase shifts without sacrificing signal amplitude.

The curve in Figure 1(b) exhibits a non-uniform concave behavior, reaching its minimum absorption coefficient at 1000 m^{-1} at the central carrier frequency of 300 GHz, and symmetrically increasing to 1000.125 m^{-1} at the band edges (295 GHz and 305 GHz). To mitigate edge fading, the frequency-dependent PRO optimization mechanism plays a pivotal role.

4.3 Performance comparison in wideband THz band

To compute the sum-rate across various transmit power levels, the proposed sub-THz STAR-RIS framework (which considers phase and amplitude coupling) is evaluated in comparison with three conventional systems. These benchmark systems include: ideal STAR-RIS (featuring ideal elements with fixed amplitude β_n = 1, traditional RIS (with elements limited to reflection-only and 180° coverage), and STAR-RIS with random phase shifts (utilizing randomized phase displacement angles).

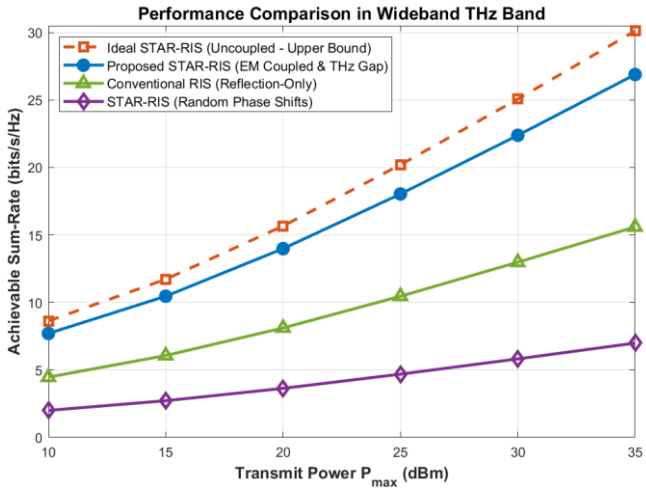


Figure 2. The relation between sum-rate and transmit power for four systems

It is observed that the sum-rate scales positively with the increase in transmit power for all four evaluated frameworks, as shown in Figure 2. Despite physical coupling constraints and atmospheric path loss, the proposed STAR-RIS scheme closely approaches the ideal baseline, achieving a narrow performance gap across the power range. Furthermore, the proposed scheme achieves an improvement in system throughput over the conventional RIS surface, demonstrating the clear advantage of full 360° simultaneous reflection and transmission coverage. Finally, the poor performance of the

random-phase baseline at 7 bits/s/Hz, this underscores the necessity for optimization of beamforming.

4.4 Extended spatial trade-off analysis: User spatial distribution vs. array size N

To evaluate the spatial adaptability and scalability of the proposed system, Figure 3 presents a comparison of the achievable sum-rate against the spatial distribution of users for different STAR-RIS array sizes ($N \in 32, 64, 128$). A fixed total number of 12 users is considered throughout the simulations. The user distribution percentage represents the proportion of users located in the reflection and transmission regions of the STAR-RIS. The horizontal axis reflects the user spatial distribution, ranging from 0% (all 12 users in the transmission region) to 100% (all 12 users in the reflection space), while 50% 12 users are equally distributed. Therefore, the total number of users remains constant, while only their spatial distribution between the two regions changes.

To comprehensively evaluate system performance under realistic blockage conditions, four comparison schemes are considered. First, the Proposed STAR-RIS ($N \in \{32, 64, 128\}$) operates under the ES protocol to enable simultaneous signal transmission and reflection while accounting for practical hardware constraints. Second, the Ideal STAR-RIS ($N = 64$) serves as an unconstrained theoretical upper bound without phase or amplitude implementation limits. Third, the Conventional RIS ($N = 64$) acts as a reflection-only benchmark to highlight the coverage advantages of full 360° spatial service. Finally, the Random Phase STAR-RIS ($N = 64$) incorporates unoptimized, randomly generated phase shifts to directly quantify the performance gains derived from the proposed DES-PRO optimization algorithm.

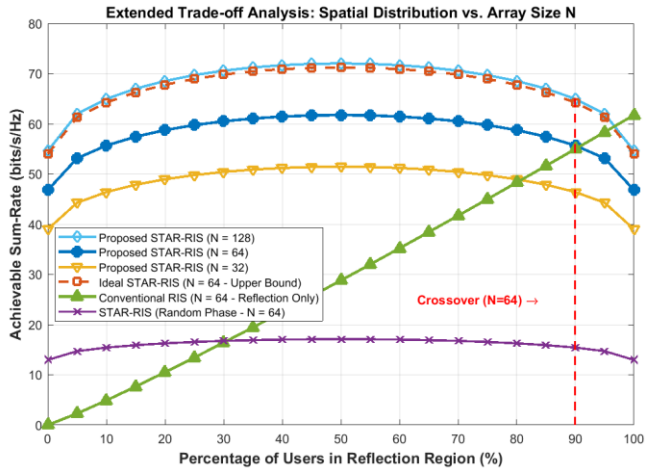


Figure 3. Impact of user spatial distribution and surface array size N on the system sum-rate performance

As shown in Figure 3, all enhanced STAR-RIS surfaces exhibit a symmetric concave behavior, reaching peak sum-rate performance when users are equally distributed between the reflection and transmission spaces 50%. Scaling the surface array size ($N = 32, 64, 128$) lead to increase sum rate, effectively offsets the atmospheric absorption losses inherent to sub-THz frequencies. Conversely, the traditional RIS exhibits a linear response; service is completely disrupted when all users reside within the transmission region. However, performance improves as users move toward the reflection region. The random-phase system maintains a near-flat, degraded sum-rate response persistently low sum rate. Ultimately, further optimizing the proposed STAR-RIS architecture remains essential to fully exploit its inherent transmission gains. The peak sum-rate throughput is achieved at the 50% spatial distribution point because the ES protocol to uniformly distributes transmit power to mitigating inter-beam interference, thereby fully exploiting the available system resources.

Consequently, we evaluated the performance of the proposed STAR-RIS framework across three surface element configurations ($N \in \{32, 64, 128\}$) alongside the three baseline systems under realistic blockage conditions. By simulating a network deployment serving 16 users, the impact of signal blockage was examined across a spectrum ranging from 0% (unobstructed LOS) to 100% (complete signal blockage). Where the blockage ratio represents the percentage of obstructed channels between the BS and the STAR-RIS, or between the STAR-RIS and the users. Furthermore, the influence of hardware coupling constraints specifically the non-linear phase-amplitude relationship was analyzed in mitigating these blockage induced impairments.

Figure 4 illustrates the achievable sum-rate as a function of the link blockage ratio for a 16-user setup. As observed, all evaluated schemes suffer from a monotonic performance degradation as the blockage ratio increases; however, the proposed STAR-RIS demonstrates exceptional resilience. At moderate blockage levels (30%–50%), performance remains relatively stable due to dynamic energy redistribution. By reallocating the transmission power toward the available channels, the DES algorithm enhances the remaining active communication links.

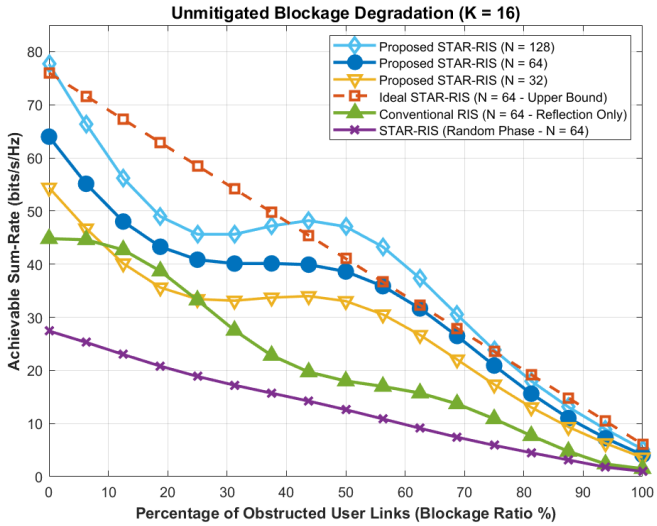


Figure 4. Impact of unmitigated link blockage on sum-rate performance for various simultaneously transmitting and reflecting reconfigurable intelligent surfaces (STAR-RIS) configurations (K = 16)

At $N = 64$, the proposed architecture maintains a robust sum rate. Conversely, conventional reflection-only RIS suffers a sharp performance collapse below 18 bits/s/Hz due to its inability to serve users in the transmission region.

To isolate the explicit algorithmic contribution framework from massive hardware gains, we evaluate benchmark optimization algorithms specifically at $N = 64$. The array size was fixed at $N = 64$ as it represents an optimal trade-off point between sum-rate throughput gains and implementation

complexity. At this surface size, unoptimized power allocation and phase shift adjustments fail around severe blockages. To overcome this challenge, we propose the DES-PRO algorithm a hybrid integration of the DES for comprehensive exploration and the PRO for joint power and phase optimization under physical coupling constraints. Figure 5 compares four optimization benchmarks: Deep Reinforcement Learning (DRL) (a data-driven model based on trial-and-error interaction with high computational complexity), Phase-Only Optimization (a conventional approach that adjusts reflection and transmission phase shifts with fixed power allocation, ignoring phase-amplitude coupling), Dynamic User Scheduling (characterized by unfairness, as it prioritizes unblocked users while denying service to users with blocked direct links), and the proposed DES-PRO algorithm.

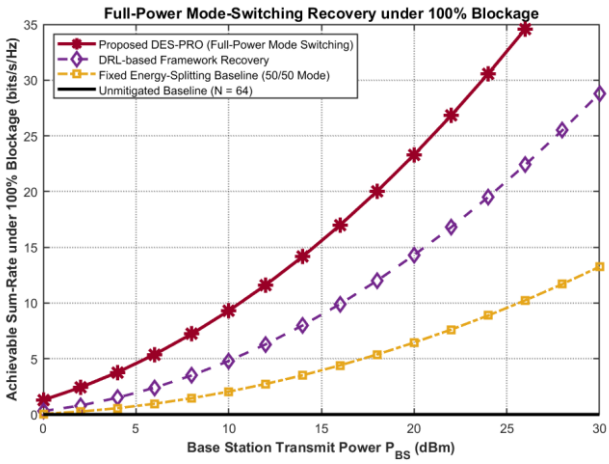


Figure 5. Sum-rate performance under varying link blockage ratios for different optimization algorithms

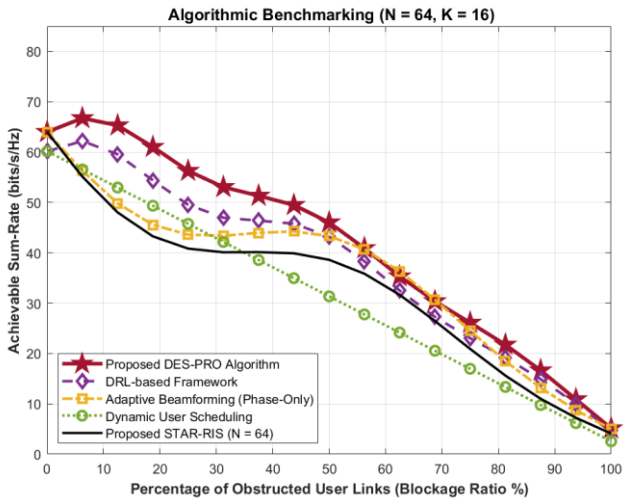


Figure 6. Sum-rate performance of full-power mode-switching recovery under complete blockage conditions

The obtained results demonstrate that the proposed DES-PRO algorithm consistently outperforms the benchmark systems. Under moderate link blockage (30%), the proposed algorithm achieves higher throughput compared with DRL, phase-only beamforming, and baseline configurations As shown in Figure 6. Furthermore, while the performance of DRL degrades as the user signal blockage ratio increases, it still exhibits robust competitive behavior relative to the proposed algorithm. Conversely, the Dynamic User Scheduling suffers a linear degradation with higher blockage ratios, which is attributed to its inability to dynamically reallocate power resources.

Due to static power allocation, the Adaptive Beamforming (phase-only) achieves a sum-rate of 44 bps/Hz under moderate blockage conditions. However, as the blockage ratio exceeds 70%, its performance suffers a rapid degradation.

4.5 Network recovery and survivability under severe 100% link blockage

To evaluate the ultimate limits of network resilience, we simulated a worst-case scenario where direct service to all users is completely blocked by obstacles. To assess the network's recovery efficiency under complete outage conditions, we incorporated a Full-Power Mode-Switching mechanism into the proposed DES-PRO algorithm. This mechanism allows the STAR-RIS elements to dynamically switch and allocate 100% of their power exclusively to either reflection or transmission based on user locations. We evaluated this recovery capability across BS transmit power levels ranging from [0, 30] dBm, comparing it against three key baseline models: DRL-based recovery, fixed 50/50 power-splitting STAR-RIS, and a conventional network operating without intelligent surfaces.

The numerical results demonstrate that the dynamic full-power mode-switching capability within the proposed $\mathcal{T}_{DES-PRO}$ algorithm serves as the optimal mechanism to overcome critical link blockages in sub-THz systems. As illustrated in Figure 5, the proposed DES-PRO algorithm targets active users exclusively by dynamically co-optimizing both phase and amplitude, thereby avoiding power dissipation across active and blocked users as observed in static 50/50 power-splitting schemes. According to the obtained results, the DES-PRO algorithm demonstrates superior effectiveness owing to its power recovery capability and its capacity to enhance overall system efficiency.

In multi-user sub-THz networks, acquiring perfect CSI is extremely challenging due to severe path loss and atmospheric absorption. To evaluate the proposed algorithm under realistic conditions, it was tested under imperfect CSI, where channel estimation error rates range from 0% (perfect CSI) to 25% (severe estimation error). The performance of the proposed DES-PRO with electromagnetic coupling was compared against the ideal uncoupled STAR-RIS upper bound and conventional reflection-only RIS surfaces.

As shown in Figure 7, the proposed DES-PRO algorithm demonstrates high resilience in the presence of channel estimation errors, suffering only a minor and gradual throughput degradation as the error rate increases. Under perfect CSI conditions (0% estimation error), the proposed algorithm closely the 57bits/s/Hz ideal baseline of the ideal uncoupled surface. Under severe estimation error conditions of the proposed algorithm maintains resilient sum rate, whereas at a 20% error rate, it matches and slightly surpasses the ideal scheme. This behavior occurs because the ideal model strictly optimizes beamforming based on noisy channel estimates without error compensation mechanisms, leading to severe beam misalignment; instead of steering an ultra-narrow beam that fails due to noise, the penalty-based regularization mechanism in the proposed algorithm absorbs estimation errors by slightly broadening the beamwidth, thereby guaranteeing link stability and strength. The conventional RIS

achieves a sum-rate of 31.8 bits/s/Hz highlighting its structural performance limitations. Ultimately, the proposed DES-PRO algorithm firmly demonstrates its robust capability to mitigate severe blockage impairments and channel deficiencies in high-frequency 5G and 6G networks.

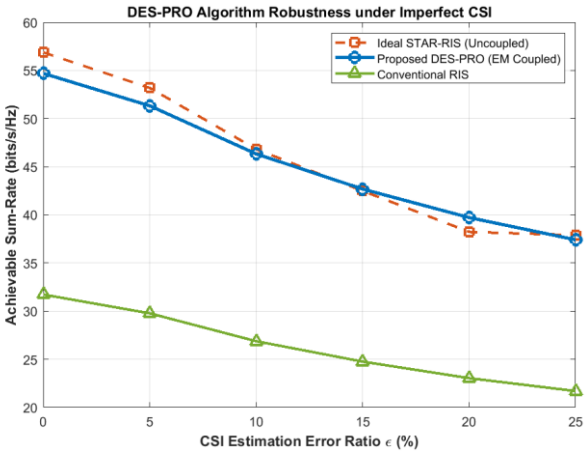


Figure 7. Impact of channel estimation error ratio ϵ (%) on the system sum-rate under imperfect channel state information (CSI)

5. CONCLUSIONS

Prior literature often assumed independent phase and amplitude controls; however, a strong practical interdependence exists between them in MU-MIMO networks, where phase shifts inherently induce amplitude variations. To address these challenges in sub-THz, a novel STAR-RIS optimization algorithm, termed DES-PRO combining DES with PRO to advance dynamic system optimization for 360° coverage.

Four distinct operational scenarios were modeled. Scenario 1 assessed the impact of scaling the array size confirming that combining simultaneous transmission and reflection with physical aperture scaling effectively offsets practical phase-amplitude coupling losses compared to conventional models.

Scenario 2 evaluated user signal blockage, where the proposed DES-PRO algorithm demonstrated clear superiority over DRL, phase-only optimization, and dynamic user scheduling schemes. Specifically, the proposed DES-PRO algorithm outperformed all benchmark approaches. Scenario 3 evaluated performance under full-power mode-switching Maintaining throughput performance under severe blockage conditions. Scenario 4 assessed system behavior under realistic imperfect environmental conditions, confirming robust efficiency. In the presence of channel estimation errors (ϵ), the simulation results demonstrate a high throughput. However, practical implementation faces several limitations, including the computational complexity of the proposed algorithm, control latency associated with the surface elements, and the need for large-scale arrays for its deployment.

REFERENCES

[1] Abdul-Wajid, O.M. (2025). AI-enhanced dynamic beamforming for high-mobility mm wave 5G networks. Journal of Advancement in Communication System, 8(2): 6-12. https://doi.org/10.5281/zenodo.15532581

[2] Abed, R.A., Ayoob, S.A. (2023). Millimeter wave beams coordination and antenna array height effect. AIP Conference Proceeding, 2830: 040003. https://doi.org/10.1063/5.0157290

[3] Rappaport, T.S., Sun, S., Mayzus, R., et al. (2013). Millimeter wave mobile communications for 5G cellular: It will work! IEEE Access, 1: 335-349. https://doi.org/10.1109/ACCESS.2013.2260813

[4] Alkhateeb, A., El Ayach, O., Leus, G., Heath, R.W. (2014). Channel estimation and hybrid precoding for millimeter wave cellular systems. IEEE Journal of Selected Topics in Signal Processing, 8(5): 831-846. https://doi.org/10.1109/JSTSP.2014.2334278

[5] Abed, R.A., Ayoob, S.A. (2022). A proposed method to coordinate mmWave beams based on coordinated multi-point in 5G networks. Journal of Communications, 17(11): 925-932. https://doi.org/10.12720/jcm.17.11.925-932

[6] Chowdhury, M.Z., Shahjalal, M., Ahmed, S., Jang, Y.M. (2020). 6G wireless communication systems: Applications, requirements, technologies, challenges, and research directions. IEEE Open Journal of the Communications Society, 1: 957-975. https://doi.org/10.1109/OJCOMS.2020.3010270

[7] ElMossallamy, M.A., Zhang, H., Song, L., Seddik, K.G., Han, Z., Li, G.Y. (2020). Reconfigurable intelligent surfaces for wireless communications: Principles, challenges, and opportunities. IEEE Transactions on Cognitive Communications and Networking, 6(3): 990-1002. https://doi.org/10.1109/TCCN.2020.2992604

[8] Alsawaf, H.A., Ayoob, S.A. (2025). Compressive channel estimation for hybrid passive/active IRS-assisted mm-Wave MIMO systems. Journal of Communications, 20(2): 166-175. https://doi.org/10.12720/jcm.20.2.166-175

[9] Ayoob, S.A., Alsharbaty, F.S., Abd, Z.S. (2026). Improving security for 6G networks using beamforming technology. ITEGAM Journal of Engineering and Technology for Industrial Applications, 12(59): 1682-1692. https://doi.org/10.5935/jetia.v12i59.3631

[10] Alsawaf, H.A., Ayoob, S.A. (2026). Deep learning for channel state information in intelligent reflecting surface-aided massive MIMO systems. Journal Européen des Systèmes Automatisés, 59(6): 1545-1556. https://doi.org/10.18280/jesa.590603

[11] Basharat, S., Khan, M., Iqbal, M., Hashmi, U.S., Zaidi, S.A.R., Robertson, I. (2022). Exploring reconfigurable intelligent surfaces for 6G: State-of-the-art and the road ahead. IET Communications, 16(13): 1458-1474. https://doi.org/10.1049/cmu2.12364

[12] Liu, Y., Mu, X., Xu, J., et al. (2022). STAR: Simultaneous transmission and reflection for 360° coverage by intelligent surfaces. IEEE Wireless Communications, 28(6): 102-109. https://doi.org/10.1109/MWC.001.2100191

[13] Xu, J., Liu, Y., Mu, X., Dobre, O.A. (2021). STAR-RISs: Simultaneous transmitting and reflecting reconfigurable intelligent surfaces. IEEE Communications Letters, 25(9): 3134-3138. https://doi.org/10.1109/LCOMM.2021.3082214

[14] Sui, Z., Ngo, H.Q., Matthaiou, M., Hanzo, L. (2025). Performance analysis and optimization of STAR-RIS-aided cell-free massive MIMO systems relying on

imperfect hardware. IEEE Transactions on Wireless Communications, 24(4): 2925-2939. https://doi.org/10.1109/TWC.2025.3526563

[15] Ge, H., Papazafeiropoulos, A., Ratnarajah, T. (2023). Impact of phase noise in downlink STAR-RIS-aided massive MIMO systems. IEEE Communications Letters, 28(2): 392-396. https://doi.org/10.1109/LCOMM.2023.3346685

[16] Li, Q., El-Hajjar, M., Sun, Y., et al. (2023). Achievable rate analysis of the STAR-RIS-aided NOMA uplink in the face of imperfect CSI and hardware impairments. IEEE Transactions on Communications, 71(10): 6100-6114. https://doi.org/10.1109/TCOMM.2023.3287995

[17] Luo, X., Jiang, Z., Xu, F., Li, X., Zhu, G., Shen, K. (2024). Sum-rate maximization for STAR-RIS-assisted multi-user networks with hardware impairments. IEEE Wireless Communications Letters, 13(5): 1503-1507. https://doi.org/10.1109/LWC.2024.3378846

[18] Wang, Z., Mu, X., Liu, Y., Schober, R. (2022). Coupled phase-shift STAR-RISs: A general optimization framework. IEEE Wireless Communications Letters, 12(2): 207-211. https://doi.org/10.1109/LWC.2022.3219020

[19] Qin, X., Song, Z., Hou, T., Yu, W., Wang, J., Sun, X. (2023). Joint resource allocation and configuration design for STAR-RIS-enhanced wireless-powered MEC. IEEE Transactions on Communications, 71(4): 2381-2395. https://doi.org/10.1109/TCOMM.2023.3241176

[20] Sui, Z., Ngo, H.Q., Matthaiou, M. (2024). STAR-RIS-aided cell-free massive MIMO with imperfect hardware. In GLOBECOM 2024-2024 IEEE Global Communications Conference, Cape Town, South Africa, pp. 5259-5264. https://doi.org/10.1109/GLOBECOM52923.2024.10901180

[21] Du, H., Zhang, J., Guan, K., et al. (2022). Performance and optimization of reconfigurable intelligent surface aided THz communications. IEEE Transactions on Communications, 70(5): 3575-3593. https://doi.org/10.1109/TCOMM.2022.3162645

[22] Abeywickrama, S., Zhang, R., Wu, Q., Yuen, C. (2020). Intelligent reflecting surface: Practical phase shift model and beamforming optimization. IEEE Transactions on Communications, 68(9): 5849-5863. https://doi.org/10.1109/TCOMM.2020.3001125

[23] Matos, S., Ma, Y., Luo, Q., et al. (2024). Reconfigurable intelligent surfaces for THz: Hardware impairments and switching technologies. In 2024 International Conference on Electromagnetics in Advanced Applications (ICEAA), Lisbon, Portugal, pp. 415-420. https://doi.org/10.1109/ICEAA61917.2024.10701743

[24] Papazafeiropoulos, A., Kourtessis, P., Chatzinotas, S. (2023). Max-min SINR analysis of STAR-RIS assisted massive MIMO systems with hardware impairments. IEEE Transactions on Wireless Communications, 23(5): 4255-4268. https://doi.org/10.1109/TWC.2023.3316707

[25] Zhang, N., Liu, Y., Mu, X., Wang, W., Huang, A. (2023). Queue-aware STAR-RIS assisted NOMA communication systems. IEEE Transactions on Wireless Communications, 23(5): 4786-4801. https://doi.org/10.1109/TWC.2023.3322381

[26] Choudhury, D., Sah, A.K. (2024). Energy efficient joint beamforming design for hardware-impaired STAR-RIS-assisted CF-mMIMO systems. IEEE Transactions on Communications, 73(6): 3849-3862. https://doi.org/10.1109/TCOMM.2024.3496716

[27] Lin, Y., Shen, Y., Li, A. (2022). Simultaneous transmission and reflection beamforming design for RIS-aided MU-MISO. IEEE Transactions on Vehicular Technology, 72(3): 4040-4045. https://doi.org/10.1109/TVT.2022.3214829

[28] Gao, Q., Liu, Y., Mu, X., Jia, M., Li, D., Hanzo, L. (2023). Joint location and beamforming design for STAR-RIS assisted NOMA systems. IEEE Transactions on Communications, 71(4): 2532-2546. https://doi.org/10.1109/TCOMM.2023.3247753

[29] Wang, T., Fang, F., Ding, Z. (2023). Joint phase shift and beamforming design in a multi-user MISO STAR-RIS assisted downlink NOMA network. IEEE Transactions on Vehicular Technology, 72(7): 9031-9043. https://doi.org/10.1109/TVT.2023.3248789

[30] Mu, X., Liu, Y., Guo, L., Lin, J., Schober, R. (2021). Simultaneously transmitting and reflecting (STAR) RIS aided wireless communications. IEEE Transactions on Wireless Communications, 21(5): 3083-3098. https://doi.org/10.1109/TWC.2021.3118225

[31] Sheng, Z., Song, Z., Yu, H., Nasir, A.A., Liu, Y. (2024). STAR-RIS-aided MISO networks with multi-user rate fairness. IEEE Communications Letters, 28(12): 2925-2929. https://doi.org/10.1109/LCOMM.2024.3481665

[32] Alqahtani, A., Taneja, N., Taneja, A., Alqahtani, N. (2025). Energy aware resource management in 6G IoT networks using STAR RIS. Scientific Reports, 15: 20941. https://doi.org/10.1038/s41598-025-05338-w

[33] Liu, Y., Mu, X., Schober, R., Poor, H.V. (2022). Simultaneously transmitting and reflecting (STAR)-RISs: A coupled phase-shift model. In ICC 2022-IEEE International Conference on Communications, Seoul, Korea, Republic of, pp. 2840-2845. https://doi.org/10.1109/ICC45855.2022.9838767

[34] Zhu, G., Mu, X., Guo, L., Huang, A., Xu, S. (2023). Robust resource allocation for STAR-RIS assisted SWIPT systems. IEEE Transactions on Wireless Communications, 23(6): 5616-5631. https://doi.org/10.1109/TWC.2023.3327502

[35] Qian, B., Qiao, J., Zhang, C. (2024). Star-RIS-assisted millimeter-wave secure communication with multiple eavesdroppers. Mathematics, 12(14): 2259. https://doi.org/10.3390/math12142259

[36] Bahingayi, E.E., Perović, N.S., Tran, L.N. (2025). On the joint beamforming design for large-scale downlink RIS-assisted multiuser MIMO systems. IEEE Transactions on Wireless Communications, 25: 4816-4832. https://doi.org/10.1109/TWC.2025.3614297

[37] Ge, H., Garg, N., Papazafeiropoulos, A., Ratnarajah, T. (2023). Transceiver design for IRS-aided massive MIMO networks with rate-splitting. IEEE Access, 11: 142162-142176. https://doi.org/10.1109/ACCESS.2023.3343612

[38] Li, H., Liu, Y., Mu, X., Chen, Y., Pan, Z., Eldar, Y.C. (2023). Near-field beamforming for STAR-RIS networks. arXiv preprint arXiv:2306.14587. https://doi.org/10.48550/arXiv.2306.14587

[39] Zhang, G., Lu, Y., Ai, B., Zhong, Z., Ding, Z., Quek, T.Q. (2023). Energy-efficient design in STAR-RIS assisted communication system with antenna selection. In GLOBECOM 2023-2023 IEEE Global Communications Conference, Kuala Lumpur, Malaysia,

pp. 637-642. https://doi.org/10.1109/GLOBECOM54140.2023.10436885

NOMENCLATURE

N	Total number of STAR-RIS elements
K	Total number of users
K_{sub}	Number of subcarriers
t	Time slot/time index
$\theta_t(t)$	Transmission response matrix of the STAR-RIS at time index t
$\theta_r(t)$	Reflection response matrix of the STAR-RIS at time index t
$\beta_{t,n}(t)$	Amplitude adjustment coefficient for the transmitted signal via the nth element at time index t
$\beta_{r,n}(t)$	Amplitude adjustment coefficient for the reflected signal via the nth element at time index t
$\beta_n^v(\phi_n^v)$	Phase dependent effective amplitude adjustment coefficient for the nth STAR-RIS element in operational mode v ∈ {t, r}
β_t	Aggregate transmission and reflection amplitude vector at time slot t
β_{min}	Minimum amplitude attenuation coefficient achieved at maximum phase dissipation
$\phi_{t,N}(t)$	Phase shift applied to the transmitted signal via the nth element at time index t
$\phi_{r,N}(t)$	Phase shift applied to the reflected signal via the nth element at time index t
$\phi(t)$	Continuous phase shift vector aggregating all transmission and reflection phase shifts across STAR-RIS elements at time slot t
ϕ_o	Circuit specific reference phase shift parameter in the physical amplitude-phase coupling model
$SINR_k(t)$	Instantaneous Signal-to-Interference-plus-Noise Ratio for user k at time t
$R_{sum}(t)$	Achievable sum-rate at time slot t
B	System bandwidth
$h_{r,k}^H$	Complex wireless channel vector between STAR-RIS surface and user k
$h_{d,k}^H$	Direct complex wireless channel vector between Base Station and user k
G	Actual aggregate complex wireless channel matrix between Base Station and STAR-RIS
$\hat{G}$	Estimated channel matrix acquired at the Base Station
ΔG	Channel estimation error matrix
$W_k(t)$	Digital beamforming vector synthesized by Base Station for user k at time slot t
$W_m(t)$	Digital beamforming vector allocated to interfering users (m = k)
δ_k^t	Additive White Gaussian Noise (AWGN) power at receiver k
P_{max}	Maximum allowable transmit power threshold at Base Station
$k_{abs}(f)$	Terahertz molecular absorption coefficient
f	Subcarrier frequency

Greek symbols

γ	Electromagnetic response steepness (curvature coefficient)
ϵ	Upper bound on allowable channel estimation error ratio (ϵ = 0.20)
α_k	Adaptive step-size parameter at iteration step k
λ	Penalty parameter in PRO algorithm
$\nabla_\phi R_{sum}$	Gradient of sum-rate objective function evaluated with respect to phase shift vector

Subscripts

k	User index (k ∈ {1, … , K})
m	Interfering user index (m = k)
n	STAR-RIS element index (n ∈ {1, …, N})
t	Transmission mode/Time index
r	Reflection mode
v	Operational mode (v ∈ {t, r})
abs	Absorption
min, max	Minimum/Maximum value
BS	Base Station
H	Conjugate transpose (Hermitian) operator
T	Transpose operator
$\|.\|_F$	Frobenius norm
$\|.\|_2$	Euclidean norm
$\|.\|$	Absolute value/scalar magnitude
$Diag(.)$	Transforms a vector into its corresponding diagonal matrix
$P_\phi(.)$	Projection operator enforcing feasible phase angle bounds
$F_{PRO}(.)$	Transformation mapping function coupling amplitude matrix with beamforming weights
$D_{EM}(.)$	Metric function measuring deviation from physical EM coupling curve
$\mathcal{T}_{DES-PRO}(.)$	Joint iterative operator of DES-PRO algorithm
j	Imaginary unit (j = $\sqrt{-1}$)